Depth-Resolved Imaging Based on Optical Sampling by Cavity Tuning

Lin Yang, *Student Member, IEEE*, and Lingze Duan, *Senior Member, IEEE*

***Abstract*— We report here a demonstration of depth-resolved optical imaging based on optical sampling by cavity tuning (OSCAT). Both optical coherence tomography and three-dimensional surface mapping are performed using an OSCAT imager. Limitations on axial resolution and pulse repetition-rate stability are discussed and viable solutions are provided. Compared with other ultrafast laser-based schemes, such as asynchronous optical sampling, OSCAT provides a simple, cost-effective solution for rapid, large-depth noninvasive imaging.**

***Index Terms*— Interferometers, laser applications, metrology, optical imaging, reflectometry, tomography, ultrafast optics.**

I. Introduction

DEPTH-RESOLVED optical imaging (DROI) allows the depth information of an object to be mapped into the time domain (i.e. time delay) and hence is able to reveal the axial structure of a sample without physically cutting through it [1]. The concept has been widely applied in biomedical imaging [2], industrial inspection [3], and non-contact profilometry [4]. Some of the most well-known DROI techniques include optical coherence tomography (OCT) [5] and three-dimensional (3D) surface mapping [6]. A critical component for DROI is tunable optical delay (TOD), which enables the scan along the axial direction (A-scan) [1]. Over the last two decades, much of the effort to improve the performance of DROI has focused on developing new TOD strategies to achieve faster A-scan with greater ranges of depth.

The most straightforward approach to achieve TOD is a mechanical delay line. The scan rate of a mechanical scan system can reach kHz level. However, there is a trade-off between scan rate and scan depth, and at its top speed, a mechanical delay line can only reach a scan depth of 2–3 mm [7]. Spectral-domain methods overcome the scan-rate limitation of mechanical delay lines with non-mechanical, wavelength-resolved detection (e.g., spectrometers) [8]–[10]. In recent years, the emergence of the swept source technology, such as Fourier domain mode locking (FDML) [11], [12] and microelectromechanically (MEMS) tuned vertical-cavity surface-emitting lasers (VCSEL) [13], [14], has further pushed the OCT axial scan rates to hundreds of KHz or even above 1 MHz. Typically, the spectral-domain methods suffer a sensitivity roll-off due to depth-dependent sensitivity loss and mirror-conjugate images [15], which limit the total imaging depth to a few millimeters [12]–[14], [16]. However, recent advance in short-cavity MEMS-VCSEL has dramatically mitigated this limitation, achieving imaging depths as large as tens of centimeters [17], [18].

Meanwhile, novel approaches based on ultrafast lasers and optical frequency combs have opened a new avenue toward high-speed, large-depth TOD [19]–[29]. Asynchronous optical sampling (ASOPS), for example, employs two femtosecond lasers with slightly detuned repetition rates and has demonstrated scan of optical delay as fast as 100 kHz with total scan ranges up to 30 cm at 10-kHz [20]. ASOPS-based OCT has achieved an imaging depth of 150 mm at an acquisition rate of several kilohertz [21]. Despite these improvements, ASOPS suffers a major drawback as it requires an additional femtosecond laser and a complex phase lock system to keep the two lasers in accordance, which add significant cost and complexity to the scheme.

To address this problem, an alternative scheme called optical sampling by cavity tuning (OSCAT) has recently been developed [23]–[29]. OSCAT aims to use one single femtosecond laser to attain similar tunable pulse relative delays as in ASOPS. The method is to add an intra-cavity modulation to tune the pulse repetition rate and let the produced pulse train go through an interferometer with highly mismatched arm lengths. The combination of the repetition-rate modulation and the path-length mismatch, as has been shown previously [24], [28], creates a scan of the relative pulse delay at the rate of the modulation. In essence, OSCAT still relies on mechanical tuning – the change of repetition rates is typically realized by varying the laser cavity length through intra-cavity piezo-electric (PZT) actuators. However, compared to the conventional mechanical delay lines, these PZT actuators have much wider bandwidths. In fact, intra-cavity PZT tuning as fast as 180 kHz has been demonstrated [30]. Moreover, it has been shown that a small variation of the cavity length may lead to a large relative pulse delay at the output of the interferometer, and this "magnification" factor can be as large as 10^3–10^4 [28]. In other words, a 10-μm PZT displacement can produce the same tuning range as a centimeter-scale optical delay line. These features make OSCAT a cost-effective solution for those applications that demand rapid, large-depth TOD.

We have previously demonstrated OSCAT-based lidar and its application in tracking dynamic motions of remote

Manuscript received April 2, 2015; revised May 21, 2015; accepted May 24, 2015. Date of publication June 1, 2015; date of current version July 10, 2015. This work was supported in part by the National Science Foundation under Grant ECCS-1040019 and in part by the Alabama EPSCoR Graduate Research Scholars Program.

The authors was with the University of Alabama in Huntsville, Huntsville, AL 35899 USA (e-mail: ly0003@uah.edu; lingze.duan@uah.edu).

Color versions of one or more of the figures in this letter are available online at http://ieeexplore.ieee.org.

Digital Object Identifier 10.1109/LPT.2015.2439613

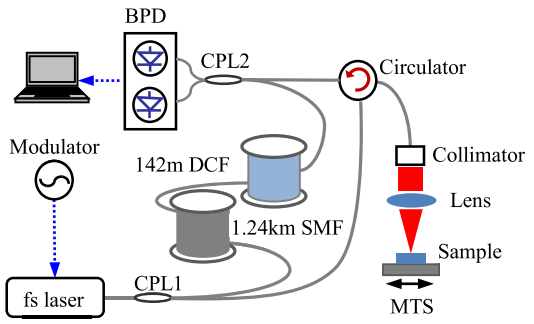

Fig. 1. A schematic layout of the OSCAT imaging system. BPD: balanced photodetector; CPL: optical coupler; DCF: dispersion compensating fiber; MTS: motorized translation stage; and SMF: single-mode fiber.

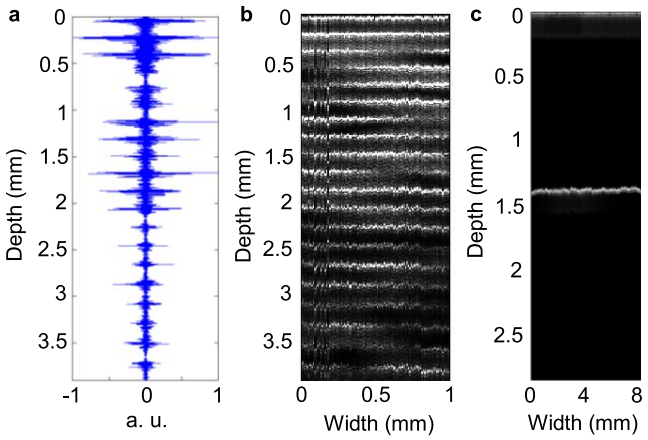

Fig. 2. (a) A typical A-scan trace obtained with a stack of 20 glass plates as the sample. (b) A two-dimensional tomographic image of the 20-layer glass-plate stack. (c) In a multi-phase sample consisting of air, oil and water, the interfaces between air and oil (top) and oil and water (middle) are revealed by the imager.

targets [28], [31]. Here, we show that OSCAT can also be used as an imaging tool to produce DROI. The motivation is to take advantage of the potentially very large (cm scale) scan depth of OSCAT, which complements the shortcomings of most time-domain and spectral-domain methods currently being used. Extending the imaging depth could open up a broader range of applications for DROI. For example, industrial process control systems often require in situ knowledge of multi-phase (i.e. gas, liquid and solid) flow inside pipelines, which is currently measured using electrical tomography methods with very poor spatial resolutions [32], [33]. Optical tomography capable of reaching enough depth could drastically improve the spatial resolution. Other DROI applications, such as 3D surface profiling, can also benefit from the extended imaging depth [6].

II. Experimental Setup

The system layout of our OSCAT imager is shown in Fig. 1. A femtosecond fiber laser (MenloSystems M-Comb) generates a near-IR (1560 nm) pulse train with a repetition rate of 250 MHz. An intra-cavity translation stage provides coarse tuning of the repetition rate by up to 2.5 MHz, and a high-speed PZT actuator, with a bandwidth of 20-kHz, allows the repetition rate to be rapidly dithered by as much as 3.55 kHz peak-to-peak. The Mach-Zehnder interferometer has two fiber arms with a length difference of 1.39 km. The long arm consists of a 1.25-km single-mode fiber followed by a 142-m dispersion compensating fiber. The optical power coupled into the long arm is about 0.5 mW and an exit pulse width of about 500 fs has been measured. The pulses from the shorter arm are launched into free space by a collimator and then focused onto the sample, which is situated on a two-axis translation stage. The stage is driven by two stepper motors controlled by a computer to make transverse scans. Light reflected off the sample is collected by the collimator and rerouted by a circulator. It is then combined with the beam from the long arm on a 2×2 coupler and coupled into a balanced photodetector. The detector probes the cross-correlations produced by the two pulse trains and a data acquisition system record the scan traces. Pulses from the long arm and the short arm are optimized separately with dispersion compensation. The resulted cross-correlation trace has a full width at half maximum (FWHM) of roughly 700 fs.

To operate our OSCAT imager, we first find the cross-correlation signal from a reference surface, which is typically a known flat surface such as the substrate of the sample. This is done by sweeping the intra-cavity stage and hence scanning the repetition rate across a relatively large range. Once this reference point is found, we fix the stage and modulate the intra-cavity PZT actuator to perform the A-scan. The maximum relative pulse delay is related to the repetition rate modulation by $\Delta l_d = (\Delta f_R/f_{R0})\Delta l_i$, where Δl_d is the pulse delay in terms of free-space length, Δf_R is the peak-to-peak variation of the repetition-rate, f_{R0} is the nominal repetition rate, and Δl_i is the arm-length mismatch of the interferometer. In our case, $\Delta f_R = 3.55$ kHz, $f_{R0} = 250$ MHz, and $\Delta l_i = 1.39$ km, which yields $\Delta l_d = 1.97$ cm. In other words, our OSCAT system is able to map structures about 1 cm deep in free space (considering round trips), which has been demonstrated in an earlier experiment [28]. This depth can be further extended by either increasing the arm-length difference Δl_i or increasing the ratio $\Delta f_R/f_{R0}$.

III. Results and Discussion

Fig. 2(a) shows a typical A-scan trace when a stack of 20 glass plates is used as the sample. Its axial scale has been converted from time delay (s) into depth (mm) following a similar calibration algorithm as detailed in [28]. Each plate has a nominal thickness of about 200 μm, which is clearly resolved by the cross-correlation peaks. The sample is then shifted transversely while the A-scan is being made, resulting in a cross-sectional image of the glass plate stack shown in Fig. 2(b). A total imaging depth of 4 mm in glass is achieved in this case. The wavy line shape is mainly due to the instability of the pulse repetition rate of the femtosecond laser. To show the versatility of our imaging scheme, we have tried different types of samples. For example, Fig. 2(c) is an OCT image of a multi-phase system consisting air, oil and water. The two interfaces between air and oil (top) and oil and water (middle) are clearly revealed by the imager.

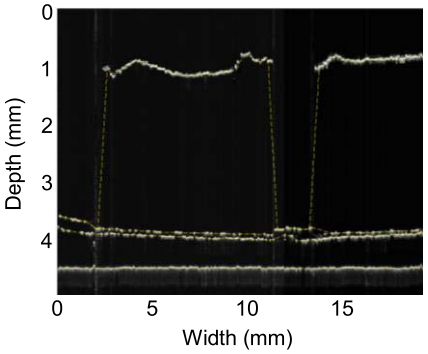

Fig. 3. An OCT image shows the cross-sectional structure of a plastic bubble foam. Two bubbles can be seen in the picture. Dashed lines are added to show the vertical walls of the bubbles. The double-layer structure of the foam bottom sheet is clearly resolved.

A more complex example is shown in Fig. 3. This is the cross-sectional structure of a plastic packing bubble foam. The foam is placed on top of a glass substrate, whose upper boundary is seen here as the continuous straight line at the bottom of the image. Two bubbles can be seen in the image (one of them is partially shown). The curvy shapes of their top layers are clearly sketched out by the scans. Since the vertical walls of the bubbles do not produce A-scan signals, dashed guiding lines are added to help readers picture the shapes of the bubbles. An air gap of about 0.5 mm is seen between the bottom of the foam and the glass substrate. The bottom sheet of the foam has a double-layer structure, which is clearly resolved by the imager. The minimum gap between the two layers is estimated to be about 100 μm.

Another important application of DROI is remote 3D surface profilometry. Combining the A-scan and a two-axis transverse scan, we have mapped the letter "H" on a UAH key chain into a 3D profile, as shown in Fig. 4(a). The key chain, which is pictured in Fig. 4(b), is mounted flat on the two-axis translation stage, and is about 5 cm away from the beam-focusing lens. The transverse scans produces an 80×72 mesh with an increment of 250 μm, and an A-scan is performed at each point on the mesh. For simple surface profiling, only the depth information is extracted from each A-scan and that leads to a 2×2 matrix of surface height and the 3D graph shown in Fig. 4(a). The sub-100-μm indent of the letter is clearly mapped out by the imager.

Two aspects about OSCAT-based DROI worth further discussion. First, the axial (or depth) resolution critically depends on the width of the pulse cross-correlation. Since the pulses from the long arm have to travel through a km-scale fiber link, dispersion compensation is crucial for maintaining a reasonable axial resolution. In our case, a simple linear dispersion compensation using dispersion compensating fibers results in a measured correlation FWHM of about 700 fs, and our imager has demonstrated the capability to resolve features as small as 100 μm. Further increase in resolution would require second- and third-order dispersion compensations, which nowadays can be routinely performed with prism- or grating-based compensators. Ultimately, the pulse width is limited by the laser. With today's femtosecond

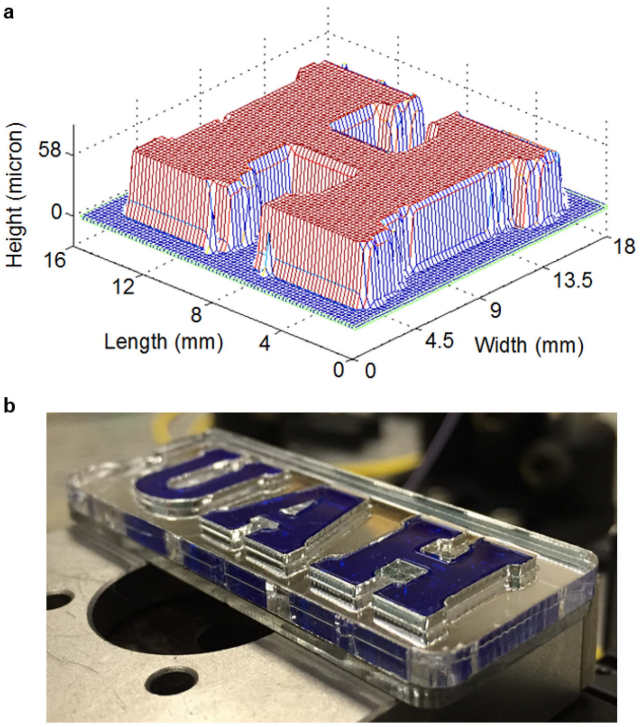

Fig. 4. (a) A 3D surface profile of the letter "H" on a UAH key chain, obtained with the OSCAT imaging system. (b) An actual picture of the key chain.

laser technology, a 10-fold improvement of axial resolution should be readily attainable. Second, a slow drift of the repetition rate is observed in our measurements, and it is attributed to the drift of the intra-cavity stage and the fluctuation of cavity length due to temperature variations. This repetition rate drift causes an artificial shift of the cross-correlation position, which is indistinguishable from the shift caused by the sample. In our data processing, the effect of this shift is removed by aligning the reflected signals from a flat reference plane (e.g., a glass surface) in all A-scan traces. Practical systems can employ an active repetition-rate control system that drives the intra-cavity stage to eliminate this slow drift. The bandwidth of this active control system will have to be much lower than the PZT modulation frequency so that the active control does not interfere with the fast repetition-rate modulation.

IV. Conclusion

In summary, we report a proof-of-principle study of OSCAT-based DROI and show that OSCAT can be a versatile technique for a breadth of imaging applications such as OCT and 3D surface profilometry. Key performance-limiting factors are discussed and feasible solutions are provided. Our scheme can serve as a cost-effective alternative to existing DROI techniques.

References

[1] C. Dunsby and P. M. W. French, "Techniques for depth-resolved imaging through turbid media including coherence-gated imaging," *J. Phys. D, Appl. Phys.*, vol. 36, no. 14, pp. R207–R227, Jul. 2003.

[2] Y. Jia, R. Nettleton, M. Rosenberg, E. Boudreau, and R. K. Wang, "Depth-resolved optical imaging of hemodynamic response in mouse brain with microcirculatory beds," *Proc. SPIE*, vol. 7898, p. 789812, Feb. 2011.

[3] M. Bashkansky, M. D. Duncan, M. Kahn, D. Lewis, III, and R. Reintjes, "Subsurface defect detection in ceramics by high-speed high-resolution optical coherent tomography," *Opt. Lett.*, vol. 22, no. 1, pp. 61–63, Jan. 1997.

[4] S. Choi, M. Yamamoto, D. Moteki, T. Shioda, Y. Tanaka, and T. Kurokawa, "Frequency-comb-based interferometer for profilometry and tomography," *Opt. Lett.*, vol. 31, no. 13, pp. 1976–1978, Jul. 2006.

[5] D. Huang *et al.*, "Optical coherence tomography," *Science*, vol. 254, no. 5035, pp. 1178–1181, Nov. 1991.

[6] E. Baumann, F. R. Giorgetta, J.-D. Deschênes, W. C. Swann, I. Coddington, and N. R. Newbury, "Comb-calibrated laser ranging for three-dimensional surface profiling with micrometer-level precision at a distance," *Opt. Exp.*, vol. 22, no. 21, pp. 24914–24928, Oct. 2014.

[7] J. Szydlo, N. Delachenal, R. Gianotti, R. Wälti, H. Bleuler, and R. P. Salathé, "Air-turbine driven optical low-coherence reflectometry at 28.6-kHz scan repetition rate," *Opt. Commun.*, vol. 154, nos. 1–3, pp. 1–4, Aug. 1998.

[8] J. F. de Boer, "Spectral/Fourier domain optical coherence tomography," in *Optical Coherence Tomography*, W. Drexler and J. G. Fujimoto, Eds. Berlin, Germany: Springer-Verlag, 2008, pp. 147–175.

[9] T. Bajraszewski, M. Wojtkowski, M. Szkulmowski, A. Szkulmowska, R. Huber, and A. Kowalczyk, "Improved spectral optical coherence tomography using optical frequency comb," *Opt. Exp.*, vol. 16, no. 6, pp. 4163–4176, Mar. 2008.

[10] N. Zhang *et al.*, "Spectral-domain optical coherence tomography with a Fresnel spectrometer," *Opt. Lett.*, vol. 37, no. 8, pp. 1307–1309, Apr. 2012.

[11] R. Huber, M. Wojtkowski, and J. G. Fujimoto, "Fourier domain mode locking (FDML): A new laser operating regime and applications for optical coherence tomography," *Opt. Exp.*, vol. 14, no. 8, pp. 3225–3237, Apr. 2006.

[12] Z. Zhi, W. Qin, J. Wang, W. Wei, and R. K. Wang, "4D optical coherence tomography-based micro-angiography achieved by 1.6-MHz FDML swept source," *Opt. Lett.*, vol. 40, no. 8, pp. 1779–1782, Apr. 2015.

[13] T.-H. Tsai *et al.*, "Ultrahigh speed endoscopic optical coherence tomography using micromotor imaging catheter and VCSEL technology," *Opt. Exp.*, vol. 4, no. 7, pp. 1119–1132, Jun. 2013.

[14] K. Liang *et al.*, "Ultrahigh speed en face OCT capsule for endoscopic imaging," *Opt. Exp.*, vol. 4, no. 7, pp. 1119–1132, Mar. 2015.

[15] R. Leitgeb, C. K. Hitzenberger, and A. F. Fercher, "Performance of Fourier domain vs. time domain optical coherence tomography," *Opt. Exp.*, vol. 11, no. 8, pp. 889–894, Apr. 2003.

[16] B. Potsaid, V. Jayaraman, J. G. Fujimoto, J. Jiang, P. J. S. Heim, and A. E. Cable, "MEMS tunable VCSEL light source for ultrahigh speed 60kHz–1MHz axial scan rate and long range centimeter class OCT imaging," *Proc. SPIE*, vol. 8213, p. 82130M, Feb. 2012.

[17] I. Grulkowski *et al.*, "Retinal, anterior segment and full eye imaging using ultrahigh speed swept source OCT with vertical-cavity surface emitting lasers," *Biomed. Opt. Exp.*, vol. 3, no. 11, pp. 2733–2751, Oct. 2012.

[18] I. Grulkowski *et al.*, "High-precision, high-accuracy ultralong-range swept-source optical coherence tomography using vertical cavity surface emitting laser light source," *Opt. Lett.*, vol. 38, no. 5, pp. 673–675, Feb. 2013.

[19] P. A. Elzinga, R. J. Kneisler, F. E. Lytle, Y. Jiang, G. B. King, and N. M. Laurendeau, "Pump/probe method for fast analysis of visible spectral signatures utilizing asynchronous optical sampling," *Appl. Opt.*, vol. 26, no. 19, pp. 4303–4309, Oct. 1987.

[20] A. Bartels *et al.*, "Ultrafast time-domain spectroscopy based on high-speed asynchronous optical sampling," *Rev. Sci. Instrum.*, vol. 78, no. 3, p. 035107, Mar. 2007.

[21] S. Kray, F. Spöler, M. Först, and H. Kurz, "Dual femtosecond laser multiheterodyne optical coherence tomography," *Opt. Lett.*, vol. 33, no. 18, pp. 2092–2094, Oct. 2008.

[22] S. Kray, F. Spöler, T. Hellerer, and H. Kurz, "Electronically controlled coherent linear optical sampling for optical coherence tomography," *Opt. Exp.*, vol. 18, no. 10, pp. 9976–9990, May 2010.

[23] T. Hochrein, R. Wilk, M. Mei, R. Holzwarth, N. Krumbholz, and M. Koch, "Optical sampling by laser cavity tuning," *Opt. Exp.*, vol. 18, no. 2, pp. 1613–1617, Jan. 2010.

[24] R. Wilk, T. Hochrein, M. Koch, M. Mei, and R. Holzwarth, "OSCAT: Novel technique for time-resolved experiments without moveable optical delay lines," *J. Infr., Millim., Terahertz Waves*, vol. 32, no. 5, pp. 596–602, Jun. 2010.

[25] R. Wilk, T. Hochrein, M. Koch, M. Mei, and R. Holzwarth, "Terahertz spectrometer operation by laser repetition frequency tuning," *J. Opt. Soc. Amer. B*, vol. 28, no. 4, pp. 592–595, Apr. 2011.

[26] A. Romann, C. Mohr, A. Ruehl, I. Hartl, and M. E. Fermann, "Mode-locked Yb-fiber laser for rapid dual pulse scanning applications," in *Proc. Adv. Opt. Mater. Conf.*, Feb. 2011, paper JWA2.

[27] S. Potvin, S. Boudreau, J.-D. Deschênes, and J. Genest, "Fully referenced single-comb interferometry using optical sampling by laser-cavity tuning," *Appl. Opt.*, vol. 52, no. 2, pp. 248–255, Jan. 2013.

[28] L. Yang, J. Nie, and L. Duan, "Dynamic optical sampling by cavity tuning and its application in lidar," *Opt. Exp.*, vol. 21, no. 3, pp. 3850–3860, Feb. 2013.

[29] S. Boudreau and J. Genest, "Range-resolved vibrometry using a frequency comb in the OSCAT configuration," *Opt. Exp.*, vol. 22, no. 7, pp. 8101–8113, Apr. 2014.

[30] T. C. Briles, D. C. Yost, A. Cingöz, J. Ye, and T. R. Schibli, "Simple piezoelectric-actuated mirror with 180 kHz servo bandwidth," *Opt. Exp.*, vol. 18, no. 10, pp. 9739–9746, May 2010.

[31] L. Yang, J. Nie, and L. Duan, "A lidar based on optical sampling by cavity tuning," in *Proc. CLEO*, Jun. 2013, paper JW2A.85.

[32] T. Dyakowski, L. F. C. Jeanmeure, and A. J. Jaworski, "Applications of electrical tomography for gas–solids and liquid–solids flows—A review," *Powder Technol.*, vol. 112, no. 3, pp. 174–192, Oct. 2000.

[33] H. S. Tapp, A. J. Peyton, E. K. Kemsley, and R. H. Wilson, "Chemical engineering applications of electrical process tomography," *Sens. Actuators B, Chem.*, vol. 92, nos. 1–2, pp. 17–24, Jul. 2003.